Biogeosciences Discuss., 10, 7831–7878, 2013
www.biogeosciences-discuss.net/10/7831/2013/
doi:10.5194/bgd-10-7831-2013

Biogeosciences Discussions
Open Access

Time-series measurements of biochemical and physical properties in the southwestern East/Japan Sea during the spring transition in 2010

Y.-T. Son[1], K.-I. Chang[1], S.-T. Yoon[1], Y.-B. Kim[2], T. Rho[3], C. K. Kang[4], and K.-R. Kim[1]

[1]Research Institute of Oceanography/School of Earth and Environmental Sciences, Seoul National University, Seoul, 151-747, Korea
[2]East Sea Research Institute, Korea Institute of Ocean Science and Technology, Uljin 767-813, Korea
[3]Department of Oceanography/Marine Research Institute, Pusan National University, Busan 609-735, Korea
[4]POSTECH Ocean Science and Technology Institute, Pohang University of Science and Technology, Pohang, 790-784, Korea

Received: 29 March 2013 – Accepted: 19 April 2013 – Published: 8 May 2013

Correspondence to: K.-I. Chang (kichang@snu.ac.kr)

Published by Copernicus Publications on behalf of the European Geosciences Union.

Abstract

An ocean buoy, UBIM, deployed during the spring transition from February and May, 2010 reveals for the first time highly-resolved temporal variation of biochemical properties of the upper layer of the Ulleung Basin in the southwestern East/Japan Sea. Meteorological data shows the typical spring transition occurred during the mooring period, weakening of wind speed, increase in shortwave radiation, and change in total heat flux from net cooling to net heating. Power spectrum of chlorophyll fluorescence (CF) peaks at semidiurnal tidal, near-inertial, diurnal, and subtidal frequencies. The diurnal variation of CF is characterized by high CF during the daytime and low CF at night. Dissolved oxygen and CF are correlated with high (low) dissolved oxygen accompanied by high (low) CF, indicating the dissolved oxygen is mainly determined by biological activities. The time series measurement captured the onset of subsurface spring bloom at 30 m, and collocated temperature and current data gives an insight into a mechanism that triggers the onset of the spring bloom not documented so far. The entire mooring period can be divided into pre-bloom period from the beginning of the mooring to early April, and bloom period afterwards. Mean CF values during the pre-bloom and bloom periods are 0.9 $\mu g\,L^{-1}$ and 1.9 $\mu g\,L^{-1}$, respectively. Mean mixed layer depth (MLD) shoaled from 22 m during the pre-bloom period to 15 m during the bloom period. Despite of the increase in shortwave radiation, average PAR values at 20 m show lower value during the bloom period as compared to that during the pre-bloom period. Low-frequency modulation of MLD ranging from 10 m to 53 m during the entire mooring period is mainly determined by shoaling and deepening of isothermal (isopycnal) depths. Temperature structure in the upper 110 m is characterized by alternating uplifting and lowering of isotherms, which is caused by the placement of the mooring site on the cold (cyclonic) or warm side of the frontal jet, the East Korean Warm Current. The frontal variability is thought to be due to the low-frequency path variatio of the East Korean Warm Current. The occurrence of the spring bloom at 30 m is concomitant with the appearance of colder East Sea Intermediate Water (ESIW) at

BGD
10, 7831–7878, 2013

buoy UBIM that results in the subsurface cooling and the shoaling of isotherms to the shallower depth levels than those occurred during the pre-bloom period. It is suggested that the springtime spreading of the ESIW is one of the important factors that triggers the onset of subsurface spring bloom below the mixed layer. The time lag between the peaks of CF and the occurrence of the shallowest isothermal depths is about several days, which appears to be the timescale for the growth of phytoplankton.

1 Introduction

The East/Japan Sea (referred to as the East Sea hereafter) is a semi-enclosed deep marginal sea in the northwestern Pacific with mean water depth of about 1800 m (Fig. 1). It comprises three deep basins deeper than 2000 m, the Japan Basin in the northern half, the Ulleung Basin to the southwest, and the Yamato Basin to the southeast. The East Sea is divided into warm water region to the south and the cold water region to the north with the subpolar front in between them. Vertical structure of the East Sea can be regarded as three layers: upper, intermediate, and deep. The upper layer corresponds to roughly upper 100 m above the main pycnocline, and contains the mixed layer and seasonal pycnocline. The intermediate and deep layers are all below the main pycnocline, or partly include the lower pycnocline. Water masses occupying the intermediate and deep layers are formed in the Japan Basin, modified, and circulate within the East Sea (Kim et al., 2004; Talley et al., 2006). On the other hand, the Tsushima Warm Water occupying the upper layer is carried by the Tsushima Current originating from the Kuroshio in the North Pacific and entering the East Sea through Korea Strait. The East Sea Intermediate Water (ESIW) characterized by a layer of shallow salinity minimum with a potential temperature range of $1 \sim 5\,^{\circ}C$ is widespread south of the subpolar front (Kim and Chung, 1984; Kim and Kim, 1999). Bimodality of the path of the ESIW in the Ulleung Basin was noted, coastal mode and offshore mode (Cho and Kim, 1994). The ESIW found offshore in the Ulleung Basin is brought into the basin through processes of subduction along the subpolar front (Kim et al., 1991;

BGD
10, 7831–7878, 2013

Lee et al., 2006), while the coastal mode refers to the path of the North Korean Cold Current carrying cold and low-salinity water originating from the Siberian coast.

The Tsushima Current bifurcates into two main branches downstream of Korea Strait. One of the branches, the East Korean Warm Current (EKWC), follows the east coast of Korea, separates from the coast at around 38° N, and meanders to the east. The meandering of the EKWC often accompanies the generation of mesoscale eddies, one of which is the quasi-permanent anticyclonic eddy called the Ulleung Warm Eddy (UWE) (Chang et al., 2004). The horizontal scale of the UWE is about 50–100 km, and it is usually found south of 37.5° N. At times, another anticyclonic eddy, called the Sokcho Eddy, is found northwest of the UWE (Kim et al., 1999).

Large-, meso-, and submesoscale physical processes and high frequency motions with varying degree of importance influence biological processes such as plankton distribution and community structure (e.g., Granata et al., 1995; McNeil et al., 1999; Wiggert et al., 2005). This is also the case for the East Sea. A comprehensive review of the pelagic ecosystem of the East Sea can be found in Lee et al. (2009).

One of the important biological features of the East Sea is the bimodality of phytoplankton bloom at the sea surface with a strong spring bloom and weak fall bloom, which have been identified mainly from satellite ocean color data (Kim et al., 2000; Yamada et al., 2004, 2005). Compilation of the satellite data further revealed large interannual and decadal variation in the timing of spring bloom (Yamada et al., 2004; Yamada and Ishizaka, 2006). Attempts have been made to explain the initiation and development of spring bloom in the East Sea using the critical depth hypothesis (Kim et al., 2000; Yamada et al., 2004; Yamada and Ishizaka, 2006), where the mixed layer depth (MLD) is the crucial physical factor for the onset of spring bloom (Sverdrup, 1953). As the shoaling of the springtime MLD was thought mainly to result from the weakening of wind and vernal warming, wind speed variation is also regarded as an important factor for the interannual variations in the initiation timings for spring bloom (Yamada et al., 2004, 2005; Kim et al., 2007). Other factors affecting the onset of spring bloom include Asian dust event (Cho et al., 2007), volume transport of the Tsushima

BGD
10, 7831–7878, 2013

Current through Korea Strait (Yoo and Kim, 2004), and location and duration of the subpolar front (Yoo and Kim, 2004). As the Tsushima Warm Water carried by the Tsushima Current is nutrient-depleted, it is suggested that large volume transport through Korea Strait inhibits the onset of spring bloom (Yoo and Kim, 2004). This argument, however, is contrary to model results which suggest the nutrient supply from the Tsushima Current through Korea Strait (Kim et al., 2013) is the main source of primary production in the Ulleung Basin (Onitsuka et al., 2007). Hence, the role of the Tsushima Current in regulating the productivity south of subpolar front is still in contention.

The annual primary production of the East Sea was estimated to be 161–222 g C m^{-2} yr^{-1} using satellite ocean color data during the 1998–2001 period (Yamada et al., 2005). Despite of the prevalence of the nutrient-depleted surface water due to the Tsushima Warm Water (Yoo and Kim, 2004), the Ulleung Basin has the highest annual primary production of 222 g C m^{-2} yr^{-1} (Yamada et al., 2005). More recent estimate of the annual primary production based on monthly water column data in the Ulleung Basin was 273.0 g C m^{-2} yr^{-1} (Kwak et al., 2013). It has been hypothesized that wind-induced coastal upwelling (Lee and Na, 1985; Park and Kim, 2010) enhances the production, and then the horizontal current, the EKWC, or the anticyclonic UWE draws the high production offshore resulting in the high productivity over the Ulleung Basin (Yoo and Park, 2009; Hyun et al., 2009). Though not mentioned explicitly, the offshore delivery of the production by large- or mesoscale horizontal advection from the coastal source region casts a doubt about the applicability of the critical depth hypothesis in controlling the spring bloom in the Ulleung Basin. Apart from the role in re-distributing the coastal production to a wider area in the Ulleung Basin, other effects of the anticyclonic UWE have been documented (Kang et al., 2004; Kim et al., 2012; Lim et al., 2012). High chlorophyll *a* concentration occurs either along the periphery of the UWE (Lim et al., 2012) or in the eddy core (Ahn et al., 2005; Kim et al., 2012).

Vertical profiles of chlorophyll *a* concentration often show a layer of the maximum chlorophyll *a* at depth in the Ulleung Basin (Shim et al., 1992; Shim and Park, 1996; Rho et al., 2010). A wide distribution of the SCM layer both in the Ulleung and Japan

BGD
10, 7831–7878, 2013

Basins has been documented (Rho et al., 2012). The SCM layer mainly observed between 30–40 m depth may last for six months in the Ulleung Basin from May to October (Rho et al., 2012). Shim et al. (1992) observed an increase in plankton cell number at the SCM in the Ulleung Basin, which suggests that the primary production at the SCM may contribute significantly to the total annual primary production in the Ulleung Basin (Rho et al., 2012). Development, duration, and evolution of the SCM, however, are poorly known.

Previous studies on the primary production and chlorophyll *a* distribution in the East Sea are based mostly on weekly or monthly composites of satellite ocean color data or sparse snapshots from survey results. Since the biological, as well as physical, processes are expected to be highly intermittent and have broad range of time scales from minutes to days and months, observations of biochemical parameters with coarse temporal resolution can cause aliasing and episodic events cannot be adequately resolved. High-resolution time series measurements of bio-optical parameters together with physical data have been conducted since the late 1980s (Dickey et al., 1991). In the East Sea, time series measurements of bio-optical parameters was conducted for the first time in 1997 near Japanese coast in the southern East Sea for about three months aiming at the verification of satellite data with a sensor package collected mostly at the surface (Ishizaka et al., 1997).

This paper reports results from the first highly-resolved time series biochemical and collocated physical data in the Ulleung Basin obtained during the spring transition in 2010. Our focus is on the temporal variation of chlorophyll fluorescence (CF) measured at 30 m, where the SCM layer has often been observed. Our study highlights a factor affecting the onset of the spring bloom at this depth, intrusion of intermediate water mass, which has not been documented so far to our knowledge.

BGD
10, 7831–7878, 2013

2 Data and processing

Ocean buoy UBIM (Ulleung Basin Integrated Mooring), equipped with physical and biochemical sensors, was deployed in the middle of the Ulleung Basin at about 2160 m depth on February 23 and recovered on 30 May 2010 (Fig. 1). Buoy UBIM biogeochemical sensors include a Water Quality Monitor (WQM, WETLabs) at 30 m, two fluorometers (ECO-FLSB, WETLabs) at 10 m and 50 m, PAR (photosynthetically active radiation) sensors (QSP-2300, Biospherical Instruments) at 10 m and 20 m, and a ISUS nitrate sensor (Johnson and Coletti, 2002) at 50 m. The WQM consists of a combination of chlorophyll fluorometer/turbidity sensor (ECO-FLNTUS), dissolved oxygen sensor (SBE 43), and conductivity/temperature/pressure sensors (SBE 52 CTD). The WQM features anti-fouling technologies, and any signature of bio-fouling was not found when the WQM was recovered.

Three temperature profilers (Aanderra TR7) were bound to the main mooring line to measure temperature from 20 m to 240 m at every 10 m interval. An additional CTD sensor (SBE 37SM) was also installed at 10 m. Surface currents are measured by an upward-looking acoustic Doppler current profiler (WHS 300, RDI) mounted at 110 m. The buoy UBIM also carried additional CTD sensors (SBE 39) and a RCM-type current meter below 230 m. Data from these deep instruments, however, are not presented here because this study focuses on the temporal variation of physical and biochemical parameters acquired in the upper 100 m within the euphotic depth.

The mooring depths of instruments in the above are all nominal depths. Measured pressure with WQM ranges from 31 dbar to 32.4 dbar with mean value of 32.1 ± 0.4 dbar, indicating little depth variation due to mooring line motion. So we do not apply any depth correction, and will use the nominal depth hereafter.

It was originally intended to deploy buoy UBIM for six months. On 21 May a research vessel visited the mooring site and found a damage of the surface buoy, and then buoy UBIM was finally recovered on 30 May. During the deployment period, the mooring seemed to be tangled with fishing net on 9 May. The sensors at 10 m were all

BGD
10, 7831–7878, 2013

damaged except the CTD sensor, and the top temperature profiler failed to record data after 9 May. Other temperature profiles were also partly malfunctioned. WQM was in good outward shape when it was recovered. Dissolved oxygen (DO) record, however, reveals a drop in mean oxygen levels after 9 May. The correlation between temperature and salinity measured by WQM was degraded also after 9 May. We did not find any visual problem in CF data until 24 May measured by WQM (Fig. 2). For data consistency, however, all data acquired after 9 May are not included in the analysis. The fluorometer at 50 m failed to record data from one week after the deployment to the end of mooring. The weekly mean CF at 50 m is about 0.1 $\mu g\,L^{-1}$, which is about 10 times smaller than CF measured at 30 m during the common length period. The nitrate sensor also malfunctioned from the beginning to 7 May due to a problem of power supply, and recorded data only about 15 days from 7 May to 22 May. Hence, nitrate data is unavailable for the analysis period from the beginning of the mooring to 9 May. Comparing the short records of CF at 30 m and nitrate at 50 m, we notice the peak-to-peak correspondence between high nitrate and CF events (not shown), suggestive of the chemical control of CF. The sampling interval for all sensors was set to be 30 min except for the nitrate sensor being sampled six times per day.

We analyze the available time series data taken from 23 February to 8 May, CF and dissolved oxygen at 30 m, PAR at 20 m, temperature data from 10 m to 110 m at every 10 m intervals, and current profiles in the upper 110 m at every 8 m intervals. Ancillary datasets are also used to interpret results from the single-point mooring: surface geostrophic currents based on AVISO sea surface height anomaly data combined with coastal sea level data (Choi et al., 2012), bimonthly serial CTD (Conductivity-Temperature-Depth) data acquired in the Ulleung Basin by National Fisheries Research and Development Institute (NFRDI) in February and April, 2010 (Fig. 1), and a zonal CTD sections along the latitude of buoy UBIM occupied on 12 and 13 May. The NFRDI survey in February was conducted in a wider area as compared to the area occupied in April (see Fig. 8). During the period of buoy UBIM deployment, meteorological data of wind, surface pressure, and air temperature are acquired at KMA

BGD
10, 7831–7878, 2013

(Korea Meteorological Agency) meteorological buoy station, which is located about 100 km distant to the northwest from buoy UBIM (Fig. 1). Net heat flux and short wave radiation data near buoy UBIM are archived from 0.5° × 0.5° gridded MERRA (Modern-Era Retrospective analysis for Research and Application) reanalysis product (http://disc.sci.gsfc.nasa.gov/daac-bin/DataHoldings.pl).

After despiking all time series data, power spectra of biogeochemical properties are examined using 30-min. interval data. Temporal variation of temperature and currents on multiple timescales have been previously documented (Chang et al., 2004; Watts et al., 2006), but the temporal variations of the biogeochemical properties have been largely unknown. A short-term variability of those properties with periods shorter than the diurnal period, however, is beyond the scope of this study as the mooring was intended to investigate the spring transition of biogeochemical properties focusing on the spring bloom. We only briefly introduce the observed diurnal pattern of CF. Time series data are then low-pass filtered with cut-off frequency of 48 h to eliminate the short-term variability. Current data are corrected for magnetic variation, decomposed into east-west (u) and north-south (v) components, and are low-pass filtered. The same filter is also applied to other time-series data including meteorological data.

The WQM, fluorometers, and nitrate and PAR sensors were all calibrated by the factory prior to the deployment. The term CF (chlorophyll fluorescence) used in this paper is regarded as the factory-calibrated chlorophyll *a* concentration ($\mu g\,L^{-1}$) according to the manufacturer (WET Labs)'s guidance. We have not acquired in situ samples enough to convert CF measured by WQM to chlorophyll concentration. During the mooring period, in situ water samples were collected at buoy UBIM only one time on 12 May and the measured in situ chlorophyll concentration at 30 m determined by the spectrophotometry was 1.2 $\mu g\,L^{-1}$, similar to the CF value of 1.1 $\mu g\,L^{-1}$ measured at the time of in situ water sampling. Although the observed CF values would not represent the in situ chlorophyll concentration, it is assumed here that the observed CF variation well represents the temporal variation of in situ chlorophyll concentration without any significant drift of CF during the mooring period.

BGD
10, 7831–7878, 2013

3 Results

3.1 Characteristics of unfiltered time series of measured parameters at 30 m

Physical and biochemical parameters measured by WQM at 30 m show temporal variability on multiple time scales with peak-to-peak ranges of 7.0 ~ 14.0 °C for temperature, 34.1 ~ 34.47 for salinity, 0.4 ~ 6.0 μg L^{-1} for CF, and 5.8 ~ 7.4 mL L^{-1} for dissolved oxygen (Fig. 2). The range of temperature and salinity correspond to the physical characteristics of the Tsushima Warm Water and the mixture between the Tsushima Warm Water and the ESIW. The CF variation is characterized by overall high values in the 2nd half of the mooring period from about 7 April. Although the period between 7 April and 8 May is referred to the bloom period in this study because of the availability of all time-series data, it should be noted that CF shows high values until 24 May. The pre-bloom period corresponds to the period before the bloom period from the beginning of the mooring. Temporal fluctuations of CF and dissolved oxygen are amplified during the bloom period.

Power spectra of CF at 30 m and v component of currents at 20 m for entire total mooring period, and pre-bloom and bloom-periods are calculated (Fig. 3a). Apart from the high spectral energy contained at periods longer than several days, power spectra of CF peak at semidiurnal tidal, local inertial, and diurnal periods, and also at periods of 2–3 days. CF spectra clearly show the amplification of temporal variations at both high- and low-frequency bands during the bloom period, which is also clear in Fig. 2. The semidiurnal spectral peak of CF is indistinct during the pre-bloom period. Another spectral peak for CF can be seen at diurnal period. Mean diurnal variation of CF for the entire and bloom periods is characterized by an increase in CF from 9.00 a.m. to 12.00 a.m., high CF (> 2.0 μg L^{-1}) between 11.00 a.m. and 18.00 p.m., and relatively low CF during the night time (Fig. 4). During the bloom period, the peak-to-peak diurnal variation ranges from 1.6 μg L^{-1} to 2.1 μg L^{-1}. The pattern and amplitude of the diurnal variation during the pre-bloom period are notably different from those during the

BGD
10, 7831–7878, 2013

bloom period. The amplitude of diurnal variation is small, and the highest CF occurs at 19.00 p.m. later than that during the bloom period.

Power spectra of current component (v) show also peaks at semi-diurnal, near-inertial, diurnal, and lower frequencies (Fig. 3b). Contrast to the spectra of CF, spectral energy difference between the pre-bloom and bloom periods is not so distinct. Spectral energy for motions shorter than about 5 h and in a period range of 1–3 days is smaller during the bloom period than during the pre-bloom period. Semidiurnal tidal currents are intensified during the bloom period as compared to those during the pre-bloom period similar to the CF spectra. On the other hand, near-inertial motions were more energetic during the pre-bloom period in winter, when wind speeds were higher than those during the bloom period (see Fig. 5, Table 1).

Visual correlation is obvious between temperature and salinity, and between CF and dissolved oxygen (Fig. 2). Both pairs of properties show statistically significant squared coherence at high and low frequencies (not shown). An increase in temperature (CF) is concomitant with an increase in salinity (dissolved oxygen) and vice versa, indicating that the dissolved oxygen content is mainly determined by biological activities at this depth level.

3.2 Atmospheric condition

Time-series of low-pass filtered meteorological parameters shows typical characteristics of atmospheric condition during the spring transition (Figs. 5 and 6). Mean wind speeds during the pre-bloom and bloom periods are 6.7 m s^{-1} and 5.8 m s^{-1}, respectively. The direction of mean winds during the two periods is also changed from north-easterly to southwesterly. (see also Table 1). Surface pressure decreases from March to May. Air temperature shows a minimum of about 2 °C on 8 March, and increased by about 16 °C on 7 May. The net surface flux is mainly positive until the end of March, meaning the net cooling, while the sea surface mainly gains heat from atmosphere from the beginning of April (Fig. 6). This change in the sign of air-sea flux was suggested to be a potential factor triggering the onset of spring bloom (Taylor and Ferrari, 2011).

BGD
10, 7831–7878, 2013

Shortwave radiation increased from March to May with low-frequency fluctuations on timescales of 4–8 days. PAR at 20 m measured at buoy UBIM shows low values from the beginning of the mooring until 9 March, and then high values between 10 March and 8 April. Short-term variability is pronounced in the 1st half of the mooring with periods short than those of shortwave radiation. After 9 April, PAR shows significantly lower values until 6 May except for a high value on 24 April. This period of low PAR values corresponds to the bloom period.

3.3 Circulation, currents, and temperature variation at buoy UBIM

3.3.1 Upper circulation in the Ulleung Basin during the mooring period

Figure 7 shows mean surface circulation of the East Sea during the buoy UBIM mooring period. Energetic surface currents occur south of 40° N characterized by the inflow of the Tsushima Current through Korea Strait, northeastward meandering of the EKWC after the separation from the east coast of Korea around 36.5° N, and mesoscale eddies. The EKWC is an extension of the Tsushima Current emanating from the western channel of Korea Strait (see Fig. 1). It flows northward hugging the east coast of Korea south of 37° N, separates from the coast to flow eastward, and turns northward at around 131° E after merging with a part of the northward flow coming from the eastern channel of Korea Strait. The separated EKWC then flows northeastward as a meandering jet, and the meander amplitude appears to be amplified downstream. Anticyclonic and cyclonic eddies are formed in crests and troughs of the meander, especially east of 133° E. Three consecutive anticyclonic eddies are found north of the EKWC meander between 37° and 40° N and west of 136° E. The eddies form counter-rotating features together with cyclonic features south of them in the troughs of the EKWC meander and also cyclonic eddies north of them. The anticyclonic eddy close to the east coast of Korea, the Sokcho Eddy according to Kim et al. (1999), was the largest with diameter greater than 100 km and most intense with maximum surface velocity of about 30 cm s^{-1}. According to the mean circulation map, buoy UBIM's location corresponds to

BGD
10, 7831–7878, 2013

the cyclonic side of the meandering EKWC. 7 day composite surface circulation maps in the Ulleung Basin during the buoy UBIM deployment period will be explained shortly, but they are generally similar to the mean current pattern shown in Fig. 7.

3.3.2 Horizontal and vertical distribution of temperature

Temperature distribution at 100 m has been thought to represent well the isopycnals, and the upper circulation of the East/Japan Sea (Ichiye and Takano, 1988). The path of the north and northeastward EKWC in Fig. 7 would mainly follow the thermal front at 100 m with warm waters to the anticyclonic side of the front. The inferred circulation from the temperature distribution at 100 m in February and April 2010 (Fig. 8) is similar to the circulation based on SSH distribution in Fig. 7. The temperature distribution in February suggests the northward flowing EKWC along the east coast of Korea, separation of the EKWC south of 37° N from the coast, followed by the meandering of the EKWC to flow northeastward. Warm water with temperature higher than 10 °C east of 131° E indicates the meandering of the EKWC. In April, the path of the EKWC shifted to the northwestward, and the warm region with temperature higher than 10 °C had been expanded south of 37° N. An isolated moderately warm water with temperature higher than 8 °C that appears west of 130.5° E and north of 37° N is due to the anticyclonic Sokcho Eddy identified also on the SSH map in Fig. 7. In April, the Sokcho Eddy moved slightly shoreward, and the maximum temperature of the eddy decreased in April.

Three regions can be identified in the Ulleuing Basin according to the horizontal distribution of temperature at 100 m in February and April: warm water region influenced by the EKWC in the southeastern and eastern basin with temperature higher than 10 °C, moderately warm water region north of 37.5° N and west of 130.5° E with temperature higher than 8 °C due to the Sokcho Eddy, and cold water regions in the mid-basin, in the coastal area, and the area east of the moderately warm water region. Thermal fronts are formed between the (moderately) warm and cold water regions. According to Fig. 8, the buoy UBIM was located in the cold water region, the cyclonic side of the front, during the NFRDI survey periods. The NFRDI data were acquired between

BGD
10, 7831–7878, 2013

20 February to 1 March and between 3 and 15 April. The temperature time series measured at buoy UBIM (Fig. 10) indicates the occurrence of the cold events during these periods of NFRDI surveys. As the path of the EKWC shifted to the northwest in April, the thermal fronts south and northeast of buoy UBIM was intensified.

Vertical profiles of temperature and salinity were collected at 4 stations from B11 near buoy UBIM to the east on 12 and 13 May. Vertical section of potential temperature shows tilting of isotherms sloping downward toward the east, implying northward currents perpendicular to the section (Fig. 9). Warm ($T > 13\,^{\circ}$C) and saline ($S > 34.3$) Tsushima Warm Water can be seen in the upper 130 m at stations B13 and B14. Salinity front occurs between station B12 and 13, and a lateral salinity layering is prominent at station B12. The presence of the ESIW with a layer of the salinity minimum ($S < 34.06$) is also obvious. During the survey, Secchi disk was lowered to estimate the euphotic depth, which was about 30 ~ 50 m at the time of the survey.

3.3.3 Time series of temperature and mixed layer depth at buoy UBIM

Figure 10 shows time series of low-pass filtered temperature and currents in the upper 110 m at buoy UBIM. Over the mooring period, temperature ranged between 1 °C to 13 °C that includes the temperature ranges of the Tsushima Warm Water ($T > 10\,^{\circ}$C) carried by the EKWC, and the ESIW ($1\,^{\circ}\text{C} < T < 5\,^{\circ}$C). Low-frequency variability of temperature with a period of about 10–15 days is obvious, characterized by uplifting and lowering of isotherms resulting in alternating cold and warm events. During the cold events, the ESIW appeared below 50 m. Based on the 5 °C water at 110 m depth, the ESIW was captured five times during the entire mooring period with its duration of 9–14 days. When the ESIW disappeared, thick warm water layers with temperature higher than 10 °C occurred in the upper 60 m with an exceptionally thick warm water layer extending down to 95 m together with maximum temperature greater than 13 °C in late April between the 4th and 5th cold events. The thickness of the ESIW measured from 110 m upward to the depth of 5 °C isotherm increased from about 28 m before 8 April to 65 m for the 4th and 5th cold events. Concomitant with the thickening of the ESIW,

BGD
10, 7831–7878, 2013

the minimum temperature of the ESIW at 110 m decreased from 3 ~ 4 °C before 8 April to 2 ~ 3 °C after 8 April.

The mixed layer depth (MLD) is defined as the depth at which temperature is 0.2 °C cooler than temperature at 10 m assuming the water column shallower than 10 m is isothermal. The temperature-based MLD shows little difference from the density-based MLD in the East Sea except at a few coastal locations (Lim et al., 2012). Thus defined MLD ranged from 11 m to 53 m during the buoy UBIM deployment period. The low-frequency modulation of the MLD is characterized by the deepening and shoaling of the MLD in association with the appearance of warm (deeper MLD) and cold (shallow MLD) events.

3.3.4 Observed low-frequency currents at buoy UBIM

Northeastward or northwestward currents were dominant at buoy UBIM during the entire mooring period (Fig. 10). Record-length mean currents at 20 m at buoy UBIM are directed to the north with mean speeds of about 10 cm s^{-1}. Low-frequency fluctuations, however, are dominant with maximum speeds of about 55 cm s^{-1} at 20 m. Temporal fluctuations of the low-pass filtered currents are mainly barotropic in the upper 100 m with reduced speeds below 60 m or 80 m. Strong currents with speeds greater than 30 cm s^{-1} persisted relatively long from 26 February to 19 March with low-frequency fluctuations of about 3–4 days. After 20 March, relatively strong currents were then observed three times, 25–28 March, 9–13 April, and 21–27 April, thus persisting about 4 ~ 7 days. The occurrence of strong currents is associated with the upper warm events. Low-frequency currents at buoy UBIM starts to strengthen near the end of cold events as temperature at 10 m sharply increases. The strong currents persist during the warm events and until the beginning of cold events. During the rest of the periods of the cold events, the upper currents remain weak. The long-lasting strong currents in February and March are also associated with the warm event ($T > 11$ °C) persisting relatively long for about 20 days.

BGD
10, 7831–7878, 2013

3.4 Mean seawater and atmospheric properties during the pre-bloom and bloom periods

Low-pass filtered CF at 30 m remained below 1.5 $\mu g\,L^{-1}$ in the first half of the mooring period from the deployment to 7 April (pre-bloom period), and sharply increased to 3.0 $\mu g\,L^{-1}$ between 7 April and 11 April (Fig. 11b). From 7 April until the end of the mooring, the CF variation was characterized by relatively high CF and large low-frequency fluctuations on timescales of about 7 ~ 20 days with a peak-to-peak amplitude ranging from 0.9 $\mu g\,L^{-1}$ to 3.3 $\mu g\,L^{-1}$ (bloom period). Table 1 summarizes mean biochemical, optical, and physical properties averaged over the pre-bloom and bloom periods.

As mentioned earlier, mean meteorological parameters during the pre-bloom and bloom periods reflect the typical spring transition of atmospheric conditions, changes in wind direction from northeasterly to southeasterly, reduction of wind speed from 6.7 $m\,s^{-1}$ to 5.8 $m\,s^{-1}$, an increase in solar radiation from 170 $W\,m^{-2}$ to 224 $W\,m^{-2}$, and reversal of the sign of net surface heat flux from 58 $W\,m^{-2}$ to −67 $W\,m^{-2}$.

Mean CF values during the pre-bloom and bloom periods are 0.9 $\mu g\,L^{-1}$, and 1.9 $\mu g\,L^{-1}$, respectively (Table 1). Hence, the mean CF became doubled during the bloom period. The maximum CF during the bloom period is 3.3 $\mu g\,L^{-1}$, while it is 1.5 $\mu g\,L^{-1}$ during the pre-bloom period. Dissolved oxygen contents at 30 m are also slightly increased during the bloom period. Although the mean solar radiation was increased during the bloom period, mean PAR value at 20 m was about halved during the bloom period.

Mean temperature at 20 m during the bloom period became slightly higher due to the occurrence of warm waters with temperature higher than 12 °C three times during the bloom period (Fig. 11). On the other hand, mean temperature at 100 m during the bloom period was lowered by 1.1 °C. Associated with the cooling of the lower layer, the mean depth of 5 °C isotherm was lifted from 87.8 m during the pre-bloom period to 71.0 m during the bloom period. The mean depth of 10 °C isotherm also slightly

BGD
10, 7831–7878, 2013

shoaled from 36.6 m to 35.3 m between the pre-bloom and bloom periods. Mean currents and kinetic energy of low-frequency currents during the bloom period are weaker than those in the pre-bloom period. The kinetic energy of high-frequency currents at 20 m, however, increased by about 10 % during the bloom period as compared to that during the pre-bloom period. The high-frequency currents here are those of high-pass filtered currents including motions with periods shorter than 21 h including local inertial period (~ 19 h). According to the current spectra in Fig. 3b, the increase in kinetic energy during the bloom period is due to the intensification of internal tidal currents.

Mean MLD was slightly reduced from the pre-bloom period (22.7 m) to the bloom periods (14.9 m). As was previously mentioned, the low-frequency variation of the MLD is mainly related to the occurrence of the warm (deeper MLD) and cold (shallow MLD) events during the entire mooring period, indicative of an importance of the advection effect in determining the MLD. Apart from the vernal warming and reduced wind speed, the shoaling of mean MLD during the bloom periods is thought to result from the uplifts of subsurface isotherms closer to the surface as compared to the uplifts that occurred during the pre-bloom period. Especially, the MLD was shallower than 15 m during the last two cold events that occurred in mid April and between the end of April and the beginning of May. During these periods, CF time-series was obtained below the surface mixed layer. The shoaling of subsurface isotherms and the lowering of the minimum temperature at 100 m suggest the buoy UBIM was under an influence of newly-arrived colder ESIW during the bloom period.

3.5 Low-frequency variation of chlorophyll fluorescence

As was mentioned earlier, CF experienced the low-frequency variability with large amplitudes during the bloom period. Two peak values of low-pass filtered CF greater than 3.0 $\mu g\,L^{-1}$ occurred on 17 April and 5 May (Fig. 11). Considering the low-frequency variation of CF with its two peak value, we divide the bloom period into three events, from 7 April to 17 April (increasing CF), from 17 April to 24 April (decreasing CF), and

BGD
10, 7831–7878, 2013

from 25 April to 5 May (re-increasing CF) to examine the CF variation more in detail in conjunction with variations of physical factors (Fig. 12).

3.5.1 Event 1 (7 April to 17 April)

CF increased from 7 April to 11 April, and experienced a sharp drop between 11 April and 12 April (Fig. 12). High CF value ($> 2.0\,\mu g\,L^{-1}$) was recovered in a day on 13 April, and persisted until the end of event 1 with a peak value of $3.3\,\mu g\,L^{-1}$ on 17 April. PAR at 20 m was relatively low during the period of event 1 with the record-length minimum value on 12 April (Fig. 11).

Temperature time series in the upper 110 m during event 1 are characterized by the appearance of about 40 m thick warm water layer ($T > 12.0\,^{\circ}C$) between 9 and 11 April. The MLD becomes 26 m thick due to the occurrence of the warm water layer. The uplift of subsurface isotherms immediately followed and the warm layer was quickly shrunk. The 10 °C isotherm reached the shallowest depth less than 20 m on 11 April from 55 m on 9 April. Afterwards, isotherms of 9 °C and those less than 9 °C gradually deepened while fluctuating vertically with a period of about 3–4 days. The 10 °C isotherm also experienced the vertical fluctuations, but it showed no distinct deepening until the end of event 1. Associated with the uplift of subsurface isotherms, the MLD shoaled to be less than 15 m during the 2nd half of event 1.

As mentioned earlier, the appearance of the warm water at the beginning of event 1 was concomitant with an initiation of strong eastward currents. Strong northward currents then followed, hence the currents turned cyclonically, while the isotherms experienced the shoaling. The low-frequency currents remained weak during the rest of the period of event 1. Horizontal advection of the warm water appears to be associated with the initial increase of CF between 9 and 11 April, while the horizontal currents were weak during the rest of the period when CF remained high with a peak value on 17 April.

Figure 13 shows the distribution of MODIS chlorophyll *a* and SSH during the periods of events 1, 2, and 3. The SSH maps represent the upper circulation and show the path

BGD
10, 7831–7878, 2013

of the EKWC, flowing northward along the coast south of 36.5° N, separation from the coast, and meandering northeastward. During its deployment period, the buoy UBIM was mainly located near or upstream of the meander trough of the separated EKWC. A cyclonic eddy feature is found near buoy UBIM with its center located northwest of buoy UBIM. The existence of the cyclonic eddy can also be seen on the horizontal temperature distribution at 100 m in April (Fig. 8). The cyclonic eddy appears to have been shrunk as the front moves northwestward approaching buoy UBIM from the beginning to the end of April, and it disappeared at the beginning of May. The anticyclonic Sokcho Eddy north of 37.5° N identified in the horizontal temperature maps at 100 m is also obvious in the SSH maps.

Surface chlorophyll distribution in the 1st half of event 1 shows a high chlorophyll band extending from the southeast coast of Korea to the northeast following approximately the 1.55 m SSH isoline along the boundary of the separated EKWC (Fig. 13a). Surface chlorophyll data is unavailable northwestern region of the separated EKWC, but a map of satellite-derived sea surface temperature on April 7 clearly shows the separation of surface warm water from the coast north of 36° N and extending to the northeast (not shown). Surface chlorophyll at buoy UBIM was directly influenced by the advection of the high surface chlorophyll. The MLD at buoy UBIM was 26 m at the time of the warm water advection, and the observed initial increase in CF at 30 m at buoy UBIM between 7 and 11 April is thought to be due to this advection of high chlorophyll originating from the coast. The reason for high CF in the coastal region is beyond the scope of this study, but may be due to coastal upwelling.

During the 2nd half of event 1, relatively high chlorophyll region appears to shift to the north of 36.5° N, especially along the coast and around the western periphery of the Sokcho Eddy (Fig. 13b). Although data is not available, the surface chlorophyll would have been also high at buoy UBIM in the 2nd half of event 1 considering the high surface chlorophyll at the proximity of buoy UBIM. The observed high chlorophyll at 30 m during the 2nd half of event 1, however, needs to be explained by other processes than the horizontal advection of high surface chlorophyll from the coast as was the

BGD
10, 7831–7878, 2013

case for the initial increase in CF at 30 m between 9 and 11 April. Because the MLD shoaled less than 15 m in the second half of event 1, CF at 30 m was below the surface mixed layer. We think the observed high chlorophyll at 30 m is associated with the uplift of isotherms resulting from the displacement of the frontal boundary due to the path variability of the EKWC. Initially buoy UBIM was directly influenced by the separated EKWC, and then it's location was placed in the cold (cyclonic) side of the front, where thermocline (and pycnocline maybe also nitracline) was shallower than the euphotic depth that is favorable to phytoplankton bloom.

Low-pass filtered CF shows a large value of 3.0 $\mu g\,L^{-1}$ at mid-night on 11 April, then sharply dropped to a local minimum value of 0.9 $\mu g\,L^{-1}$ at around noon on 12 April, and increased to 2.7 $\mu g\,L^{-1}$ at 18:30 on 13 April. The timing of the abrupt decrease and re-increase of CF corresponds to the rapid shift of the location of buoy UBIM from the warm side to the cold side of the thermal front, and also to the shift from the eastward strong currents to the northward currents. The reason for the short-term abrupt variation of CF at 30 m is unclear, and it might reflect the patchiness of the phytoplankton. The incoming solar radiation showed relatively low values on 10 and 11 April. PAR measured at 20 m start to decrease on 8 April and dropped to the record-length minimum value on 12 April. The poor light condition might be also partly responsible for the short-term variability.

3.5.2 Event 2 (18–24 April)

After the 1st peak on 17 April, CF decreased gradually until April 24. Temperature structure during event 2 is characterized by the re-emergence of the warm water layer with temperature higher than 12 °C similar to that during the 1st half of event 1, but now with longer duration and deep-reaching structure. The warm water ($T > 12.0$ °C) first appeared on 20 April and was observed until 25 April at 10 m. The warm water layer thickened, and the maximum thickness of the warm layer reached 75 m on 23 April. MLD deepened from about 12 m on 21 April to 51 m on 23 April, and then shoaled again less than 20 m on 25 April.

BGD
10, 7831–7878, 2013

Strong eastward currents were observed from 21 April when the warm water layer started to deepen, which persisted until 23 April and then strong northward currents followed. The appearance of the warm water layer concomitant with strong eastward currents followed by strong northward currents is similar to those occurred in the 1st half of event 1. The CF variation, however, is different each other. CF increased when the warm layer was observed in the 1st half of event 1, while the appearance of the warm layer during the period of event 2 is accompanied by a decrease in CF.

Surface chlorophyll in the coastal region west of 130.5° E and south of 37.5° N decreased during the period of event 2 as compared to that during event 1 (Fig. 13c). Comparing the SSH maps between the events 1 and 2, the path of the EKWC slightly shifted to the north (for example, see the 1.55 cm SSH contour line in Fig. 13c), the northeastward meander amplitude of the EKWC became reduced, and cyclonic eddies seen near the trough of the meander were shrunk. The high surface chlorophyll band along the outer edge of the separated EKWC cannot be seen in event 2, because surface chlorophyll in the coastal area south of 37.5° N was low. The comparison of the surface chlorophyll distributions between the periods of events 1 and 2 supports the previous works on the importance of the coastal source of high chlorophyll and the role of horizontal advection either by large- or mesoscale circulation in making the Ulleung Basin the most productive region in the East Sea (Hyun et al., 2009; Yoo and Park, 2009). Without the coastal source, the EKWC carries nutrient-depleted water mass, and this explains the different effects of the EKWC advection observed at buoy UBIM during the periods of events 1 and 2.

North of 37.5° N, surface chlorophyll remained relatively high. It is interesting to note that the surface chlorophyll was high around the rim of the Sokcho Eddy north of 37.5° N in the 2nd half of event 1 (Fig. 13b), while surface chlorophyll was high inside the eddy in event 2.

BGD
10, 7831–7878, 2013

3.5.3 Event 3 (25 April–5 May)

After a local minimum of CF less than 0.9 $\mu g\,L^{-1}$ on 24 April, CF slightly increased to 1.4 $\mu g\,L^{-1}$ on 26 April and then decreased again to 1.0 $\mu g\,L^{-1}$ on 28 April. Then CF increased almost monotonically from 28 April to 5 May to reach the 2nd CF peak ($> 3.0\,\mu g\,L^{-1}$). CF decreased after 5 May, but it should be noted that actually CF showed also another large values around mid-May (Fig. 2).

The warm surface water seen during the period of event 2 disappeared and isotherms uplifted again reaching to the shallowest depth on 28 April. The uplifted isotherms remained shallow until 5 May when the 2nd CF peak occurred, and started to deepen afterwards concomitant with the thickening and re-emergence of warm water with temperature higher than 12.0 °C on 8 May. The strong northward currents ceased on 28 April, and low-frequency currents were generally weak when the subsurface isotherms remained shallow. The peak CF values for both event1 and 3 occurred several days (6 days for event 1 and 7 days for event 3) after the subsurface isotherms uplifted and reached to the shallowest depth levels.

4 Discussion

The time series measurement reported here highlights the importance of the springtime advection of the ESIW in triggering the subsurface phytoplankton bloom. The observed subsurface cooling at buoy UBIM during the bloom period is thought to be due to the southward spreading of the ESIW. Cooling at 100 m depth from February to April, 2010 was widespread in the Ulleung Basin except two regions affected by the Sokcho Eddy in the northwestern basin and by the separated EKWC in the southern and southeastern periphery of the basin (Fig. 14a).

Basin-averaged bi-month climatological mean temperature at 100 m and 200 m also shows temperature decrease from February and April, suggesting that the subsurface cooling observed in April 2010 was not anomalous but represents a mean feature

BGD
10, 7831–7878, 2013

(Fig. 15). Modeling investigation of seasonal variation of the volume transport of the North Korean Cold Current (coastal mode of the ESIW according to Cho and Kim, 1994) shows an increase in the transport from winter to spring with a secondary maximum transport in March (Kim et al., 2009). Mean temperature at 100 m slightly increases from April to June, and decrease again from June to August followed by an increase from August to December at 100 m and to February at 200 m. Annual minimum temperature at both 100 and 200 m occurs in August as was noted by previous works (Cho and Kim, 1994).

We note that temperature at 100 m in April 2010 (also in February 2010, not shown) was anomalously low in the central part of the Ulleung Basin as compared to the climatological mean temperature distribution (Fig. 14b). The appearance of the anomalously cold waters in 2010 could be due to the offshore shift of the EKWC path or the spreading of anomalously cold ESIW in winter and spring 2010 or both. During the winter of 2009/2010, unusually low temperatures were recorded over much of northern Eurasia and North America that are closely associated with the strongly negative phase of the Arctic Oscillation since 1950 (Wang et al., 2010). The ESIW is known to be formed north of the subpolar front, and brought into the Ulleung Basin after subducting along the subpolar front or carried by the North Korean Cold Current along the east coast Korea. During the severe winter, surface waters north of the subpolar front would be cooled below average, and then the colder ESIW spreading to the south would contribute to the observed cold anomaly in the Ulleung Basin in February and April 2010. We have not looked into the reason for this anomalously low temperature of the ESIW in April 2010 exhaustively because it is beyond the scope of this study. In any case, the climatological seasonal variation of temperature at 100 m (Fig. 15) indicates the springtime southward spreading of the ESIW to the Ulleung Basin, and the moored observation at buoy UBIM strongly suggests that the spreading of the ESIW is closely related to the initiation of the subsurface spring bloom in the Ulleung Basin.

The reason for the low-frequency fluctuations of the depth of isotherms observed at buoy UBIM is interpreted to result from the movement of the thermal front that is

BGD
10, 7831–7878, 2013

formed along the path of the EKWC. The slanted isotherms shown in Fig. 9 would be displaced laterally associated with the path variability of the EKWC after its separation from the coast. The observed strengthening and weakening of horizontal currents at buoy UBIM during the transitional periods of the lateral displacement of the fronts supports this interpretation. The low-frequency fluctuations of isothermal depths, however, could be also due to vertical advection. We roughly estimated magnitudes of horizontal and vertical velocity scales from the temperature equation neglecting the diffusion. The horizontal temperature gradient is estimated from the vertical section of temperature taken on 12 and 13 May shown in Fig. 9 by calculating temperature difference at 100 m depth between station B11 and B14 which is about 83 km apart. Magnitudes of the local temperature variation and the vertical gradient of temperature are estimated at 100 m depth using temperature time series obtained on 8 May at buoy UBIM. The required velocity scales are estimated assuming the respective horizontal and vertical temperature advection alone balances the observed time variation of temperature at buoy UBIM. With magnitudes of each term in the temperature equation, $\partial T/\partial t \sim 9.6 \times 10^{-6}\,^{\circ}\mathrm{C\,s^{-1}}$, $\partial T/\partial \times \sim 9.6 \times 10^{-5}\,^{\circ}\mathrm{C\,m^{-1}}$, $\partial T/\partial z \sim 0.045\,^{\circ}\mathrm{C\,m^{-1}}$, the order of magnitudes of the horizontal and vertical velocity becomes O ($10\,\mathrm{cm\,s^{-1}}$) and O ($2.1 \times 10^{-2}\,\mathrm{cm\,s^{-1}}$) or O ($17\,\mathrm{m\,day^{-1}}$), respectively. The estimated horizontal velocity scale is comparable to the observed velocity. The vertical velocity scale is also comparable to that occurs at the frontal region (Velez-Belchi and Tintore, 2001), suggesting that both the horizontal and vertical advection can result in the observed fluctuations of isothermal depths at buoy UBIM. Horizontal and vertical velocities are also estimated for one more case based on horizontal temperature gradient data from NFRDI acquired between 3 and 15 April (Fig. 8b) and data from buoy UBIM between 12 and 13 April when the temporal variation of temperature was relatively sharp, yielding an order of magnitudes of about $30\,\mathrm{cm\,s^{-1}}$ for horizontal velocity and $1.2 \times 10^{-2}\,\mathrm{cm\,s^{-1}}$ for vertical velocity similar to the results in the above.

Vertical velocity in the upper ocean is associated with the wind-induced Ekman pumping, meso- (e.g., McGillicuddy et al., 1998) and submesoscale features (e.g.,

BGD
10, 7831–7878, 2013

Mahadevan and Tandon, 2006), and unstable fronts (e.g., Martin and Richards, 2001). We examined the Ekman pumping, and found little indication of the enhanced upwelling during the bloom period at buoy UBIM although an area of positive wind stress curl was expanded during the bloom period as compared to that during the pre-bloom period (not shown). Along the unstable frontal jets, simultaneous upwelling and downwelling zones occur (Lima et al., 2002). As buoy UBIM was located near the crest of the meandering EKWC and also southeastern periphery of a cyclonic mesoscale eddy during the mooring period, vertical advection could also play a role in transporting nutrients upward, hence could contribute to the observed bloom at 30 m.

During the bloom period, mean kinetic energy of high-frequency currents was larger than that during the pre-bloom period (Table 1). And spectral analysis indicates internal tidal currents became more energetic in the bloom period (Fig. 3b). Hence, the enhanced internal tides may also contribute to the onset of spring bloom (e.g., Sharples et al., 2007), which is under investigation.

Warming and a decrease in the dissolved oxygen contents of deep waters have been one of main issues on regional climate changes in the East Sea (e.g., Kim et al., 2004), which is attributed to changes in the ventilation system of the East Sea (Kang et al., 2004). The cessation of deep water formation was replaced with the sinking of surface waters to shallower depth levels (Postlewaite et al., 2005; Jenkins, 2008). Various factors can influence the timing and intensity of phytoplankton bloom as previous studies suggested. The implication of the present study is that the structural change in the water mass formation due to climate change would also result in changes in the ecosystem. Especially, an increase in the formation of the ESIW in the Japan Basin might enhance the subsurface bloom in the Ulleung Basin.

Limitations of the present study are recognized, using the scarcity of biological data on phytoplankton species, zooplankton grazing, vertical structure of chlorophyll layer together with poorly resolved spatial distribution of physical parameters at the frontal region. In general, diatoms are most dominant species in the Ulleung Basin with an average of 40 % of their contribution to the total chlorophyll *a* concentration, but their

BGD
10, 7831–7878, 2013

monthly proportions show a wide range from 16 to 82 % (Kwak et al., 2013). Numerical modeling works and well-designed observation are required to better understand the interactions between the onset of the spring bloom and the frontal jet together with biological factors in this highly productive Ulleung Basin of the East Sea.

5 Summary

Time series measurement of biochemical, optical, and physical parameters at buoy UBIM in the center of the deep Ulleung Basin of the East Sea between February and May in 2010 revealed, for the first time, the highly-resolved simultaneous temporal variation of those parameters ranging from tidal periods to seasonal transition. This paper focuses on the low-frequency variation of those parameters, especially CF measured at 30 m, after eliminating tidal and inertial motions. The mooring nicely captures the onset of subsurface phytoplankton bloom in spring, allowing us to identify an important physical factor in triggering the spring bloom in the basin which has not yet been documented.

The entire mooring period can be divided into pre-bloom period before between 23 February and 7 April and bloom period from 8 April to 8 May. Mean CF during the bloom period is twice higher than that during the pre-bloom period. Comparing the mean condition between the pre-bloom and bloom periods, the bloom period is characterized by weaker wind speed, larger solar radiation, negative net heat flux (net heating), and shoaling of MLD from 22.7 m to 14.9 m. The condition appears to support the critical-depth hypothesis (Sverdrup, 1953), where the shoaling of MLD is important for the onset of the spring bloom. The MLD difference between two periods, however, is small, and collocated temperature and ancillary data strongly suggest the importance of the horizontal displacement of fronts in determining MLD possibly together with the vernal warming and reduced wind speed.

The observed temperature variation in the upper 110 m is typified by the alternating warm and cold events, each of which lasts for about several days. Vertical displacement

BGD
10, 7831–7878, 2013

of isotherms is accompanied by those events with the maximum uplifting of isotherms of about 100 m for the 10° isotherm. Horizontal distributions of temperature and SSH indicate the buoy UBIM was located near the frontal boundary of the EKWC, which hugs the east coast of Korea after entering into the East Sea through Korea Strait, separates from the coast south of 36.5° N, and meanders northeastward. The observed shoaling of isotherms at buoy UBIM occurred when buoy UBIM was placed on the cold (cyclonic) side from the warm side of the front. When buoy UBIM was placed near the front, strong currents were observed. The lateral displacement of the front is thought mainly to result from the low-frequency path variation of the EKWC. Observed low-frequency currents at buoy UBIM supports this interpretation. The time scale of the frontal variability is about 7–14 days, and it is not obvious what caused this frontal variability.

The upward and downward vertical displacement of isotherms occurred during the entire mooring period including the pre-bloom period. During the bloom period, the southward spreading of the newly formed ESIW from the region north of the subpolar front lowered subsurface temperature and resulted in further shoaling of the isotherms during the cold events with the shallower MLD less than 15 m. Hence, the uplifting of isotherms to the shallower depths as compared to that in the pre-bloom period due to the influence of the ESIW is closely associated with the observed onset of bloom at 30 m. The time lag between the peaks of CF and the occurrence of the shallowest isothermal depths is about several days, which appears to be the timescale for the growth of phytoplankton. The maximum correlation between the nitrate supply and measured Chl *a* was found with a time lag between 6 and 10 days in Southern California Bight (Omand et al., 2012).

Acknowledgements. We thank to captains and crews of R/Vs *Eardo* and *Tamsa-II* for their support during the deployment and recovery of buoy UBIM. We also thank to B. J. Choi to provide SSH data. K. J. Lee, J. H. Park, U. J. Jung helped with preparation of figures. This work was supported by Ministry of Land, Transport and Maritime Affairs, Korea through “East Asian Seas Time-series (EAST-I)” program.

BGD
10, 7831–7878, 2013

References

Ahn, Y.H., Shanmugam, P., Chang, K.-I., Moon, J.E., and Ryu, J.H.: Spatial and temporal aspects of phytoplankton blooms in complex ecosystems off the Korean coast from satellite ocean color observations, Ocean Sci. J., 40, 67–78, 2005.

Chang, K.-I., Teague, W. J., Lyu, S. J., Perkins, H. T., Lee, D.-K., Watts, D. R., Kim, Y.-B., Mitchell, D. A., Lee, C. M., and Kim, K.: Circulation and currents in the southwestern East/Japan Sea: overview and review, Progr. Oceanogr., 61, 105–156, 2004.

Cho, C. O., Lee, J.-Y., Park, K.-A., Kim, Y. H., and Kim, K.-R.: Asian dust initiated early spring bloom in the northern East/Japan Sea, Geophys. Res. Lett., 34, L05602, doi:10.1029/2006GL027395, 2007.

Cho, Y.-K. and Kim, K.: Two modes of salinity-minimum layer water in the Ulleung Basin, La Mer, 32, 271–278, 1994.

Choi, B.-J., Byun, D.-S., and Lee, K.-H.: Satellite-altimeter-derived East Sea surface currents: Estimatiuon, description and variability pattern, The Sea, J. Korean Soc. Korea, 17, 225–242, 2012.

Dickey, T., Marra, J., Granata, T., Langdon, C., Hamilton, M., Wiggert, J., Siegel, D., and Bratkovich, A.: Concurrent high resolution bio-optical and physical time series observations in the Sargasso Sea during the spring of 1987, J. Geophys. Res., 96, 8643–8663, 1991.

Granata, T., Wiggert, J., and Dickey, T.: Trapped, near-inertial waves and enhanced chlorophyll distributions, J. Geophys. Res., 100, 20793–20804, 1995.

Hyun, J. H., Kim, D., Shin, C.-W., Noh, J.-H., Yang, E.-J., Mok, J.-S., Kim, S.-H., Kim, H.-C, and Yoo, S.: Enhanced phytoplankton and bacterioplankton production coupled to coastal upwelling and an anticyclonic eddy in the Ulleung Basin, East Sea, Aquat. Microb. Ecol., 54, 45–54, 2009.

Ichiye, T. and Takano, K.: Mesoscale eddies in the Japan Sea, La Mer, 26, 69–79, 1988.

Ishizaka, J., Asanuma, I., Ebuchi, N., Fukushima, H., Kawamura, H., Kawasaki, K., Kishino, M., Kubota, M., Masuko, H., Matsumura, S., Saitoh, S., Senga, Y., Shimanuki, M., Tomii, N., and Utashima, M.: Time series of physical and optical parameters off Shimane, Japan, during fall of 1993: First observation by moored optical buoy system for ADEOS data verification, J. Oceanogr., 53, 245–258, 1997.

Jenkins, W. J.: The biogeochemical consequences of changing ventilation in the Japan/East Sea, Mar. Chem., 108, 137–147, 2008.

BGD
10, 7831–7878, 2013

Johnson, K. S. and Coletti, L. J.: In situ ultraviolet spectrophotometry for high resolution and long-term monitoring of nitrate, bromide and bisulfide in the ocean, Deep-Sea Res. I, 49, 1291–1305, 2002.
Kang, J. H., Kim, W.-S., Chang, K.-I., and Noh, J.-H.: Distribution of plankton related to the mesoscale physical structure within the surface mixed layer in the southwestern East Sea, Korea, J. Plankton Res., 26, 1515–1528, 2004.
Kwak, J. H., Lee, S. H., Park, H. J., Choy, E. J., Jeong, H. D., Kim, K. R., and Kang, C. K.: Monthly measured primary and new productivities in the Ulleung Basin as a biological "hot spot" in the East/Japan Sea, Biogeosciences Discuss., 10, 2127–2158, doi:10.5194/bgd-10-2127-2013, 2013.
Kim, D., Yang, E .J., Kim, K. H., Shin, C.-W., Park, J., Yoo, S., and Hyun, J. H.: Impact of an anticyclonic eddy on the summer nutrient and chlorophyll a distribution in the Ulleung Basin, East Sea (Japan Sea), ICES J. Marine Science, 69, 23–29, 2012.
Kim, H., Yoo, S., and Oh, I. S.: Relationship between phytoplankton bloom and wind stress in the sub-polar frontal area of the Japan/East Sea, J. Mar. Syst., 16, 205–216, 2007.
Kim, K. and Chung, J. -Y.: On the salinity minimum layer and dissolved oxygen-maximum layer in the East Sea (Japan Sea), in: Ocean Hydrodynamics of the Japan and East China Seas, edited by: Ichiye, T., Elsevier Science Publisher, 55–65, 1984.
Kim, K., Kim, K.-R., Chung, J. Y., and Yoo, H. S.: Characteristics of physical properties in the Ulleung Basin, J. Oceanol. Soc. Korea, 26, 83–100, 1991.
Kim, K., Kim, K.-R., Kim, Y.-G., Cho, Y.-K., Kang, D.-J., Takematsu, M., and Volkov, Y.: Water mass and decadal variability in the East Sea (Sea of Japan), Progr. Oceanogr., 61, 157–174, 2004.
Kim, S.-K., Chang, K.-I., Kim, B., and Cho, Y.-K.: Contribution of currents to the N abundance in the Northwestern Pacific marginal seas, Geophys. Res. Lett., 40, 143–148, 2013.
Kim, S. Y., Lee, H. S., Min, D., and Yoon, H.-J.: Comparison of nonlinear 1 1/2-layer and 2 1/2-layer numerical models with strong offshore winds and the Tsushima Current in the East Sea, Environ. Sci., 3, 91–103, 1999.
Kim, Y.-G. and Kim, K.: Intermediate waters in the East/Japan Sea, J. Oceanogr., 55, 123–132, 1999.
Kim, Y. H., Chang, K.-I., Park, J. J., Park, S. K., Lee, S.-H., Kim, Y.-G., Jung, K. T., and Kim, K.: Comparison between a reanalyzed product by 3-dimensional variational assimilation tech-

BGD
10, 7831–7878, 2013

nique and observations in the Ulleung Basin of the East/Japan Sea, J. Mar. Syst., 78, 249–264, 2009.
Kim, S. W., Saitoh, S. I., Ishizaka, J., Isoda, Y., and Kishino, M.: Temporal and spatial variability of phytoplankton pigment concentrations in the Japan Sea derived from CZCS images, J. Oceanogr., 56, 527–538, 2000.
Lee, C. M., Thomas, L. N., and Yoshikawa, Y.: Intermediate water formation at the Japan/East Sea subpolar front, Oceanography, 19, 110–121, 2006.
Lee, J. C. and Na, J. Y.: Structure of upwelling off the southeast coast of Korea, J. Oceanol. Soc. Korea, 20, 6–19, 1985.
Lee, J.-Y., Kang, D.-J., Kim, I.-N., Rho, T., Lee, T., Kang, C.-K., and Kim, K.-R.: Spatial and temporal variability in the pelagic ecosystem of the East Sea (Sea of Japan): A review, J. Mar. Syst., 78, 288–300, 2009.
Lim, J.-H., Son, S., Park, J.-W., Kwak, J.H., Kang, C.-K., Son, Y. B., Kwon J.-N., and Lee, S. H.: Enhanced biological activity by an anticyclonic warm eddy during early spring in the East Sea (Japan Sea) detected by the Geostationary Ocean Color Satellite, Ocean Sci. J., 47, 377–385.
Lima, I. D., Olson, D. B., and Doney, S. C.: Biological response to frontal dynamics and mesoscale variability in oligotrophic environments: Biological production and community structure, J. Geophys. Res., 107, doi:10.1029/2000JC000393, 2002.
Mahadevan, A. and Tandon, A.: An analysis of mechanism for submesoscale vertical motion at ocean fronts, Ocean Model., 14, 241–256, 2006.
Martin, A. P and Richards, K. J.: Mechanisms for vertical nutrient transport within a North Atlantic mesoscale eddy, Deep-Sea Res. II, 48, 757–773, 2001.
McGillicuddy, D. J., Robinson, A. R., Siegel, D. A., Jannasch, H. W., Johnson, R., Dickey, T. D., McNeil, J., Michaels A. F., and Knap, A. H.: Influence of mesoscale eddies on new production in the Sargasso Sea, Nature, 394, 263–266, 1998.
McNeil, J. D., Jannasch, H. W., Dickey, T. D., McGillicuddy, D. J., Brzezinski, M., and Sakamoto, C. M.: New chemical, bio-optical and physical observations of upper ocean response to the passage of mesoscale eddy off Bermuda, J. Geophys. Res., 104, 15537–15548, 1999.
Omand, M. M., Feddersen F., Guza, R. T., and Franks, P. J. S.: Episodic vertical nutrient fluxes and nearshore phytoplankton blooms in Southern California, Limnol. Oceanogr., 57, 1673–1688, 2012.

BGD
10, 7831–7878, 2013

Onitsuka, G., Yanagi, T., and Yoon, J.-H.: A numerical study on nutrient sources in the surface layer of the Japan Sea using a coupled physical-ecosystem model, J. Geophys. Res., 112, C05042, doi:10.1029/2006JC003981, 2007.

Park, K.-A. and Kim, K.-R.: Unprecedented coastal upwelling in the East/Japan Sea and linkage to long-term large-scale variation, Geophys. Res. Lett., 37, L09603, doi:10.1029/2009GL042231, 2010.

Postlewaite, C. F., Rohling, E. J., Jenkins, W. J., and Walker, C. F.: A tracer study of ventilation in the Japan/East Sea, Deep-Sea Res. II, 52, 1684–1704, 2005.

Rho, T., Kim, Y.-B., Park, J. I., Lee, Y.-W., Im, D. H., Kang, D.-J., Lee, T., Yoon, S.-T., Kim, T.-H., Kwak, J.-H., Park, H. J., Jeong, M. K., Chang, K.-I., Kang, C.-K., Suh, H.-L., Park, M., Lee, H., and Kim, K.-R.: Plankton Community Response to Physico-Chemical Forcing in the Ulleung Basin, East Sea during Summer 2010, Ocean Polar Res., 32, 269–289, 2010 (in Korean with English abstract).

Rho, T., Lee, T., Kim, G., Chang, K.-I., Na, T., and Kim, K.-R.: Prevailing subsurface chlorophyll maximum (SCM) layer in the East Sea and its relation to the physic-chemical properties of water masses, Ocean Polar Res., 34, 413–430, 2012 (in Korean with English abstract).

Sharples, J., Tweddle, J. F., Green, J. A. M., Palmer, M. R., Kim, Y.-N., Hickman, A. E., Holligan, P. M., Moore, C. M., Rippeth, T. P., Simpson, J. H., and Krivtsov V.: Spring-neap modulation of internal tide mixing and vertical nitrate fluxes at a shelf edge in summer, Limnol. Oceanogr., 52, 1735–1747, 2007.

Shim, J. H. and Park, J. K.: Primary production system in the southern waters of the East Sea, Korea III. Vertical distribution of the phytoplankton in relation to chlorophyll maximum layer, J. Korean Soc. Oceanogr., 31, 196–206, 1996.

Shim, J. H., Yeo, H. G., and Park, J. K.: Primary production system in the southern waters of the East Sea, Korea I. Biomass and productivity, J. Korean Soc. Oceanogr., 27, 91–100, 1992.

Son, S., Platt, T., Bouman, H., Lee, D., and Sathyendranath, S.: Satellite observation of chlorophyll and nutrients increase induced by Typhoon Megi in the Japan/East Sea, Geophys. Res. Lett., 33, L05607, doi:10.1029/2005GL025065, 2006.

Sverdrup, H.U.: On condition for the vernal blooming of phytoplankton, Journal du Conseil International pour l'Exploration de la Mer, 18, 287–295, 1953.

Talley, L. D., Min, D.-H., Lobanov, V. B., Luchin, V. A., Ponomarev, V. I., Salyuk, A. N., Shcherbina, A. Y., Tishchenko, P. Y., and Zhabin, I.: Japan/East Sea water masses and their relation to the sea's circulation, Oceanography, 19, 32–49, 2006.

BGD
10, 7831–7878, 2013

Taylor, J. R. and Ferrari R.: Shutdown of turbulent convection as a new criterion for the onset of spring phytoplankton bloom, Limnol. Oceanogr., 56, 2293–2307, 2011.
Velez-Belchi P. and Tintore J.: Vertical velocities at an ocean front, Sci. Mar., 65, 291–300, 2001.
Wang, C., Liu, H., and Lee, S.-K.: The record-breaking cold temperatures during the winter of 2009/2010 in the Northern Hemisphere, Atmos. Sci. Lett., 11, 161–168, 2010.
Watts, D. R., Wimbush, M., Tracey, K. L., Teague, W. J., Park, J.-H., Mitchell, D. A., Yoon, J.-H., Suk, M.-S., and Chang, K.-I.: Currents, Eddies, and a "Fish Story" in the southwestern Japan/East Sea, Oceanography, 19, 64–75, 2006.
Wiggert, J. D., Hood, R. R., Banse, K., and Kindle, J. C.: Monsoon-driven biogeochemical processes in the Arabian Sea, Progr. Oceanogr., 65, 176–213, 2005.
Yamada, K. and Ishizaka, J.: Estimation of interdecadal change of spring bloom timing in the case of the Japan Sea, Geophys. Res. Lett., 33, L02608, doi:10.1029/2005GL024792, 2006.
Yamada, K., Ishizaka, J., Yoo, S., Kim, H. C., and Chiba, S.: Seasonal and interannual variability of sea surface chlorophyll *a* concentration in the Japan/East Sea (JES), Progr. Oceanogr., 61, 193–211, 2004.
Yamada, K., Ishizaka, J., and Nagata, H.: Spatial and temporal variability of satellite estimated primary production in the Japan Sea from 1998 to 2002, J. Oceanogr., 61, 857–869, 2005.
Yoo, S. and Kim, H. C.: Suppression and enhancement of the spring bloom in the southwestern East Sea/Japan Sea, Deep-Sea Res. II, 51, 1093–1111, 2004.
Yoo, S. and Park, J.: Why is the wouthwest the most productive region of the East Sea/Sea of Japan, J. Mar. Syst., 78, 301–315, 2009.

BGD
10, 7831–7878, 2013

Table 1. Mean values of parameters for pre-bloom and bloom periods. Negative sign of net heat flux means net heating. High-frequency currents are those for high-pass filtered currents with cut-off frequency of 21 h.

Parameters		Pre-bloom period	Bloom period
Wind speed ($m\,s^{-1}$)		6.7	5.8
Shortwave radiation ($W\,m^{-2}$)		169.6	224.0
Net heat flux ($W\,m^{-2}$)		57.9	−67.1
Chlorophyll fluorescence at 30 m ($\mu g\,L^{-1}$)		0.9	1.9
Dissolved oxygen at 30 m ($mL\,L^{-1}$)		6.3	6.5
PAR at 20 m ($\mu E\,m^{-2}\,s^{-1}$)		29	15
Mixed layer depth (m)		22.7	14.9
Temperature at 20 m (°C)		10.7	10.9
Temperature at 100 m (°C)		4.7	3.6
Depth of 10° isotherm (m)		36.6	35.3
Depth of 5° isotherm (m)		87.8	71.0
Current at 20 m ($cm\,s^{-1}$)		16.6	14.4
Current at 100 m ($cm\,s^{-1}$)		9.4	7.9
Kinetic energy of	20 m	316.0	268.0
low-frequency currents ($cm^2\,s^{-2}$)	100 m	90.0	62.0
Kinetic energy of	20 m	202.2	216.0
high-frequency currents ($cm^2\,s^{-2}$)	100 m	75.0	65.0

BGD
10, 7831–7878, 2013

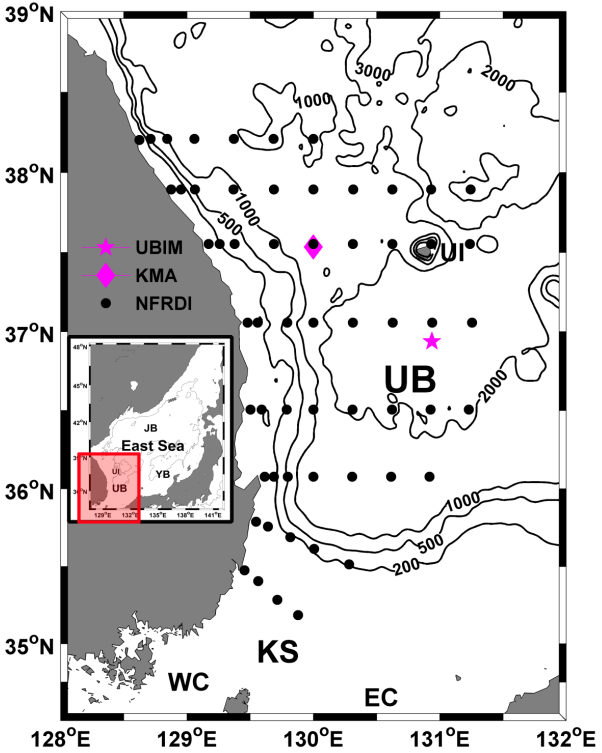

Fig. 1. Locations of buoy UBIM (star), meteorological buoy station (KMA, diamond) operated by the Korea Meteorological Agency, and bi-monthly serial oceanographic stations occupied by National Fisheries Research and Development Institute (circles) in the Ulleung Basin of the southwestern East Sea. Contours are isobaths of 200, 500, 1000, 2000, and 3000 m. UB, JB, YB, KS, WC, EC, and UI denotes the Ulleung Basin, Japan Basin, Yamato Basin, Korea Strait, eastern and western channels of Korea Strait, and Ulleungdo Island.

BGD
10, 7831–7878, 2013

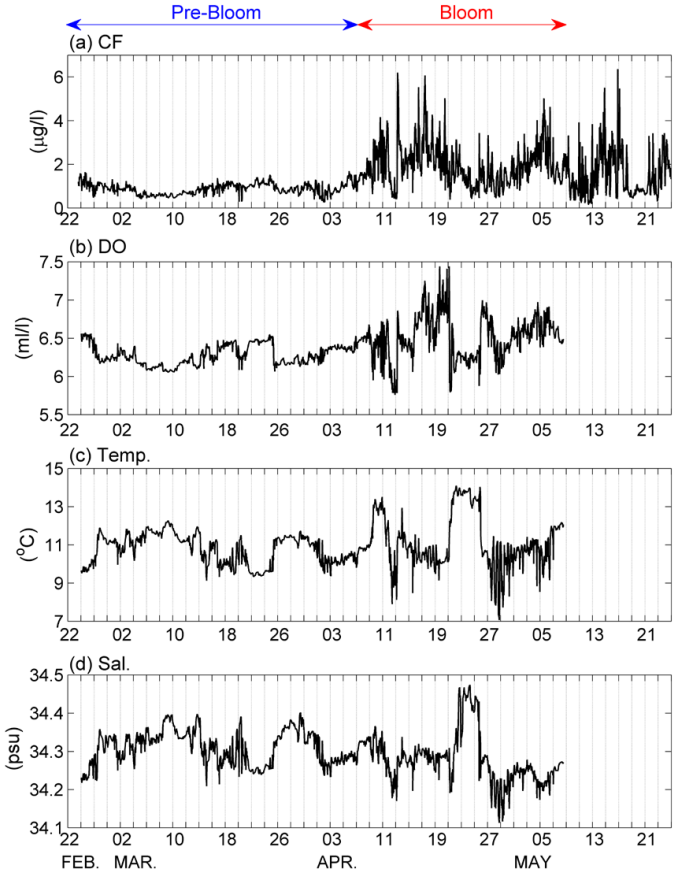

Fig. 2. Time-series of unfiltered **(a)** chlorophyll fluorescence, **(b)** dissolved oxygen, **(c)** temperature, and **(d)** salinity at 30 m measured by WQM.

BGD
10, 7831–7878, 2013

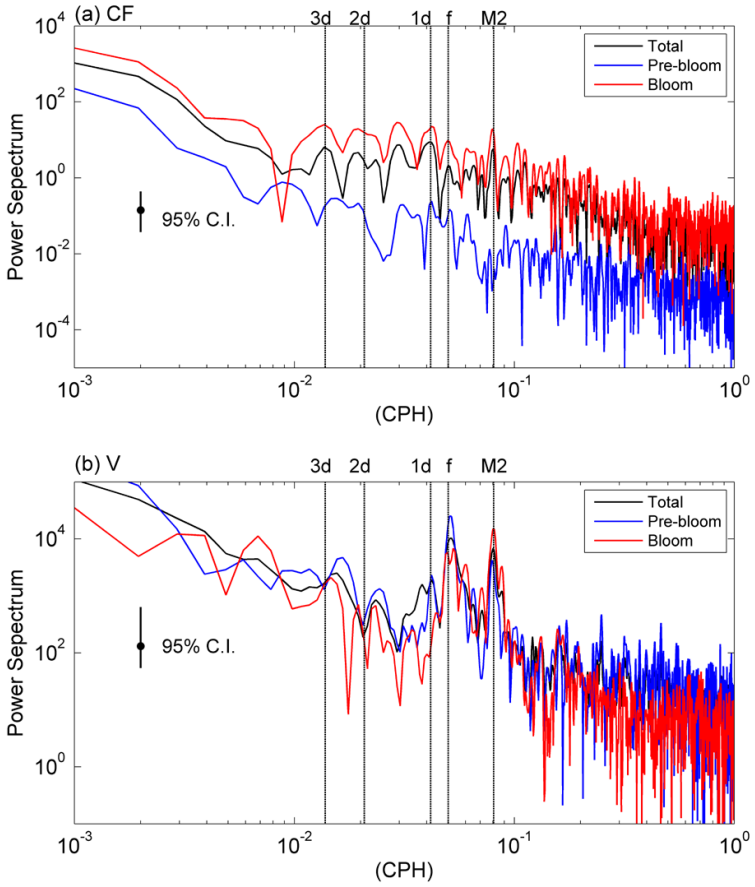

Fig. 3. (a) Power spectra of unfiltered **(a)** chlorophyll fluorescence and **(b)** north-south component of current at 20 m with data obtained during the entire mooring period (black), during the pre-bloom period (blue), and during the bloom period. Confidence level indicated by the vertical bar corresponds to 95 % significance level.

BGD
10, 7831–7878, 2013

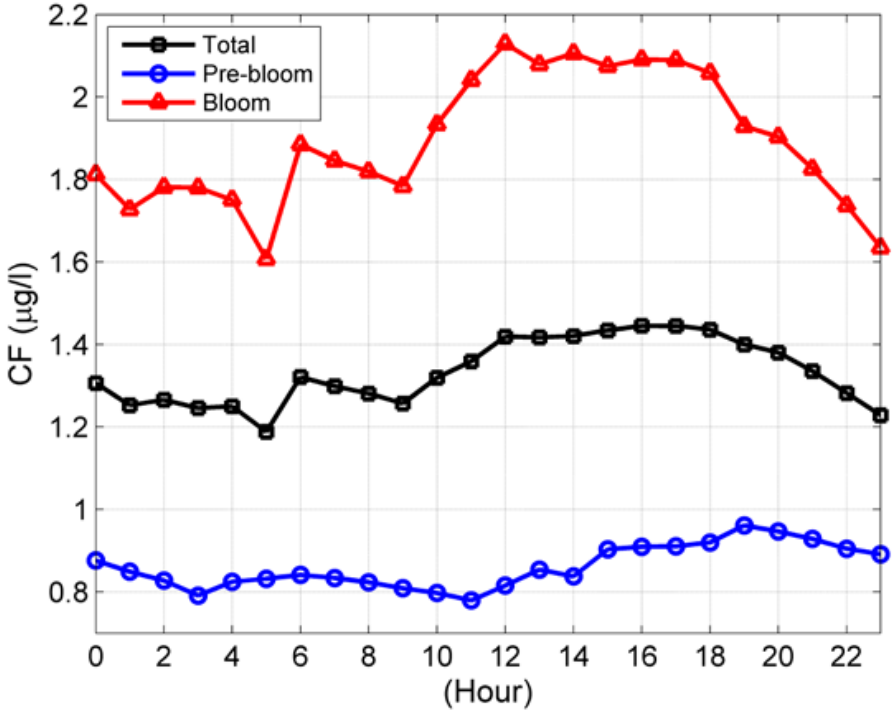

Fig. 4. Mean hourly variation of chlorophyll fluorescence based on unfiltered data for the entire mooring period (black), the pre-bloom period (blue), and the bloom period (red).

BGD
10, 7831–7878, 2013

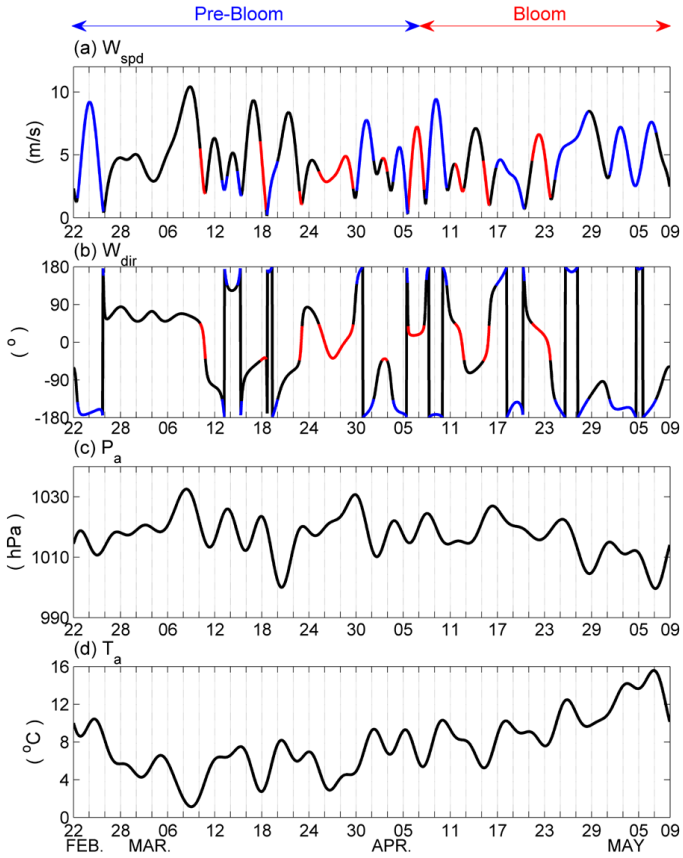

Fig. 5. Time-series of low-pass filtered **(a)** wind speed, **(b)** wind direction, **(c)** surface pressure, and **(d)** air temperature measured at KMA buoy station during the buoy UBIM deployment. Red and blue lines in **(a)** and **(b)** denote the wind speed and direction for the northerly (wind blowing from ±45° from the north) and southerly (wind blowing from ±135° from the north), respectively.

BGD
10, 7831–7878, 2013

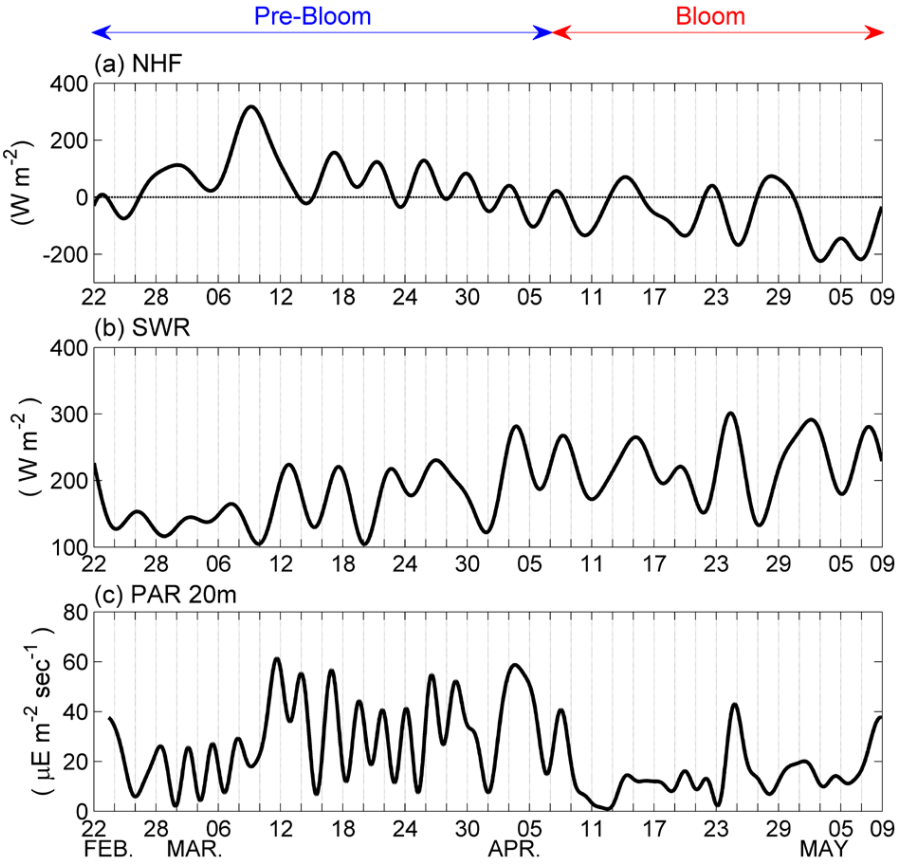

Fig. 6. Time-series of low-pass filtered **(a)** net heat flux, **(b)** shortwave radiation, and **(c)** PAR at 20 m below the sea surface during the buoy UBIM deployment. The shortwave radiation and net heat flux data at buoy UBIM are obtained from the atmospheric reanalysis product, MERRA (Modern-Era Retrospective analysis for Research and Application).

BGD
10, 7831–7878, 2013

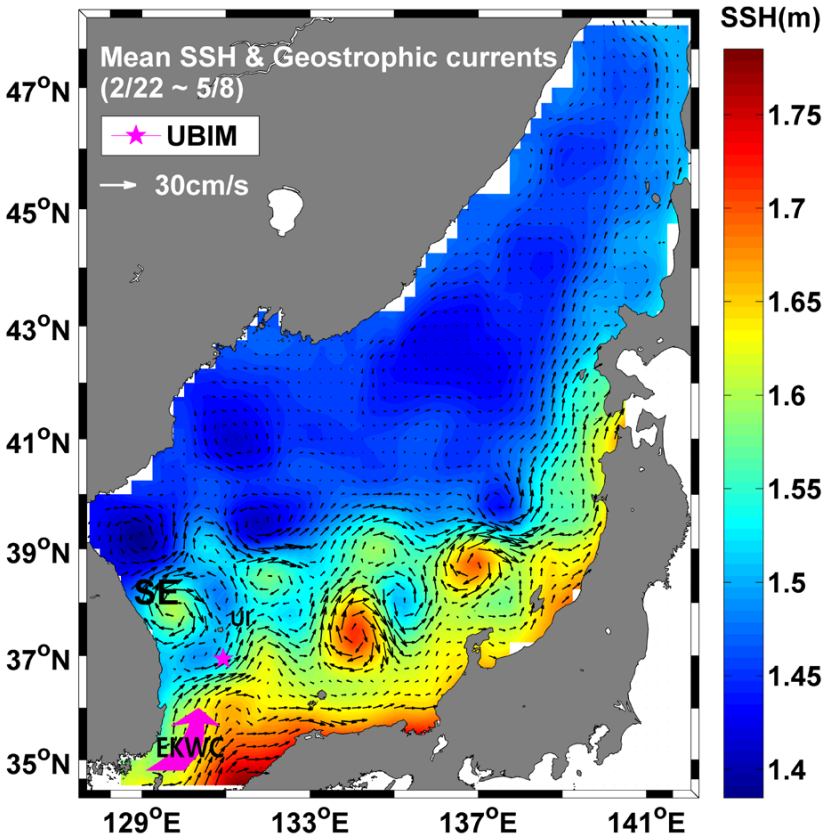

Fig. 7. Mean surface geostrohic currents and sea surface height in the East Sea during the deployment of buoy UBIM (star) calculated from satellite altimeter data combined with coastal sea level data (Choi et al., 2012). EKWC and SW denote the East Korean Warm Current and the Sokcho Eddy, respectively.

BGD
10, 7831–7878, 2013

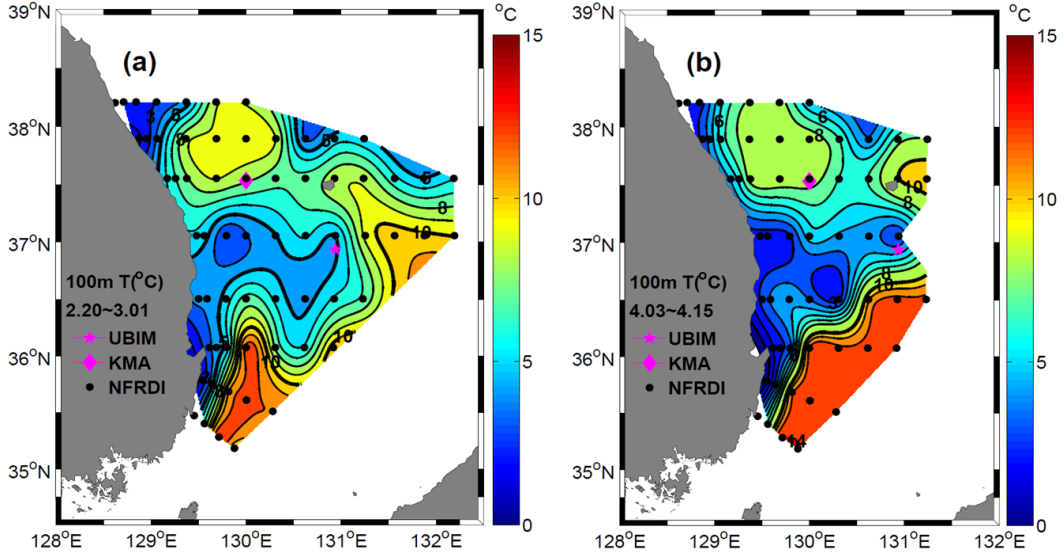

Fig. 8. Temperature distributions at 100 m in the Ulleung Basin in **(a)** February and **(b)** April, based on NFRDI bi-monthly data acquired in 2010.

BGD
10, 7831–7878, 2013

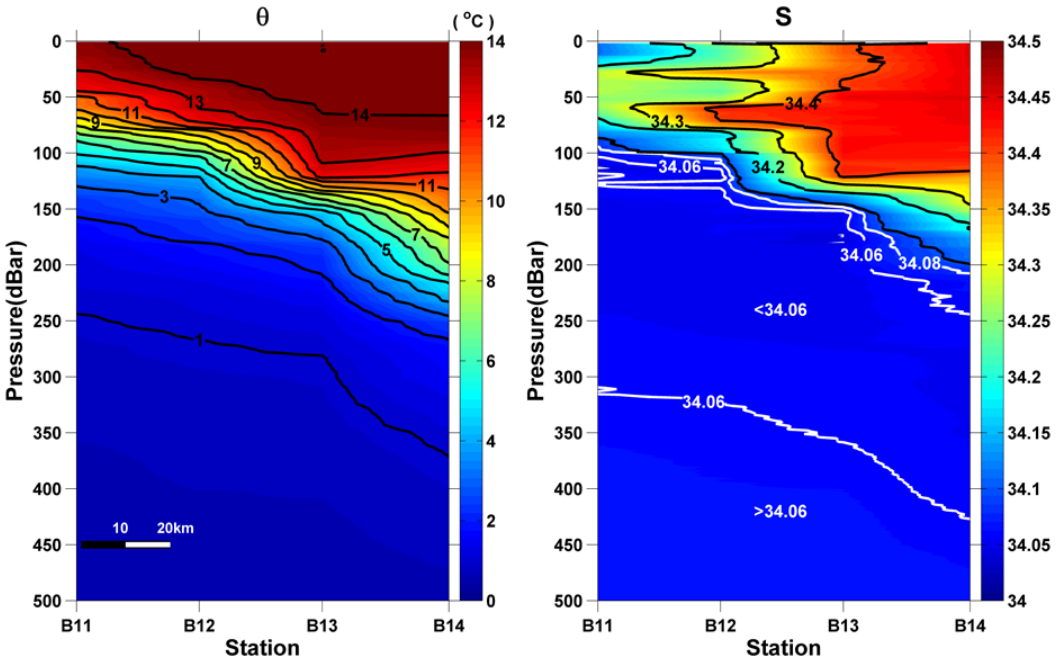

Fig. 9. Vertical distribution of temperature and salinity along a zonal section occupied on 12 and 13 May 2010. Buoy UBIM was located near station B11.

BGD
10, 7831–7878, 2013

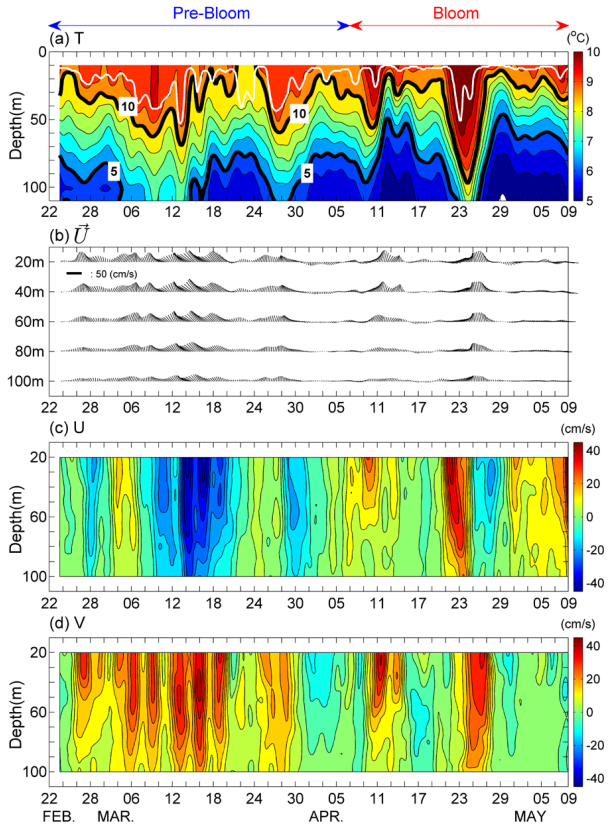

Fig. 10. Low-pass filtered time-series of **(a)** temperature, **(b)** vector currents, **(c)** east-west component (u), and **(d)** north-south component (v) in the upper 110 m at buoy UBIM. Bold lines in **(a)** indicate 5 °C and 10 °C isotherms. Mixed layer depth is shown in white lines in **(a)**. See the text for the definition of mixed layer depth.

BGD
10, 7831–7878, 2013

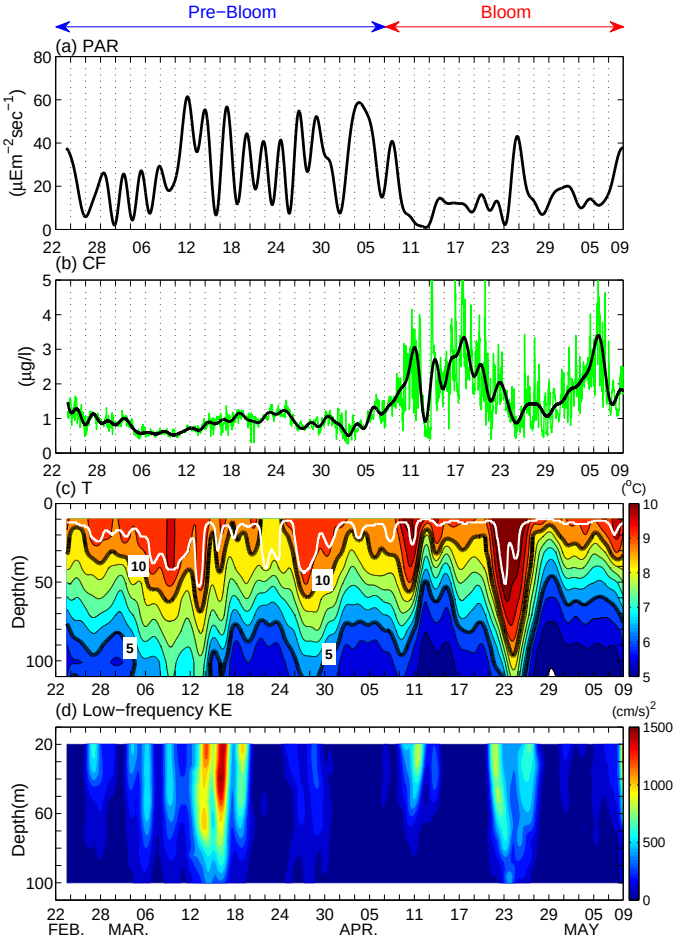

Fig. 11. Low-pass filtered time-series of **(a)** PAR at 20 m, **(b)** chlorophyll fluorescence at 30 m, **(c)** temperature in the upper 110 m, and kinetic energy of **(d)** low-frequency currents.

BGD
10, 7831–7878, 2013

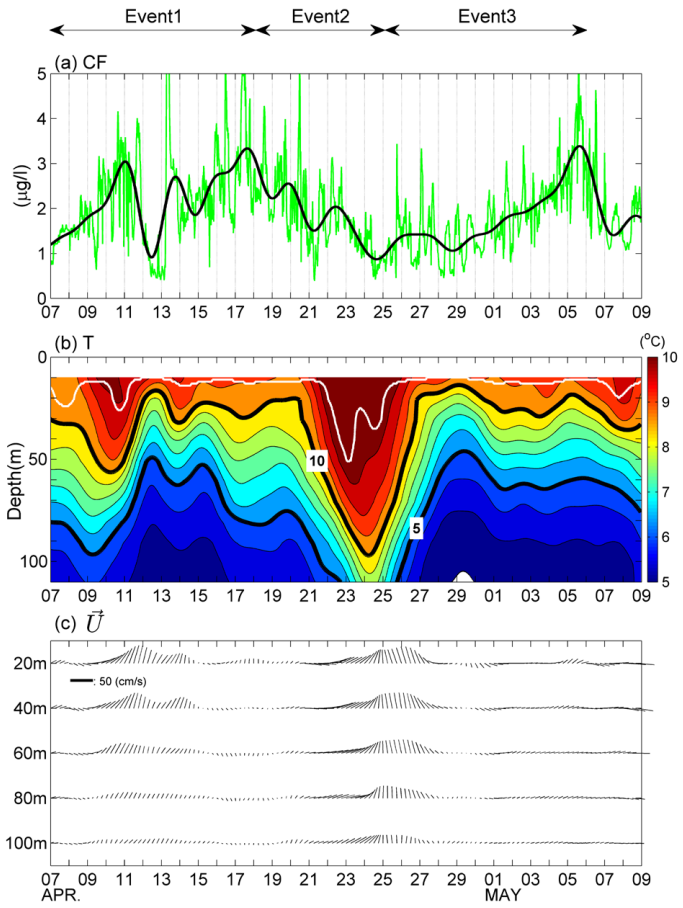

Fig. 12. Time-series of low-pass filtered **(a)** chlorophyll fluorescence at 30 m, **(b)** temperature in the upper 110 m, and **(c)** currents during the bloom period. Periods of three events are shown.

BGD
10, 7831–7878, 2013

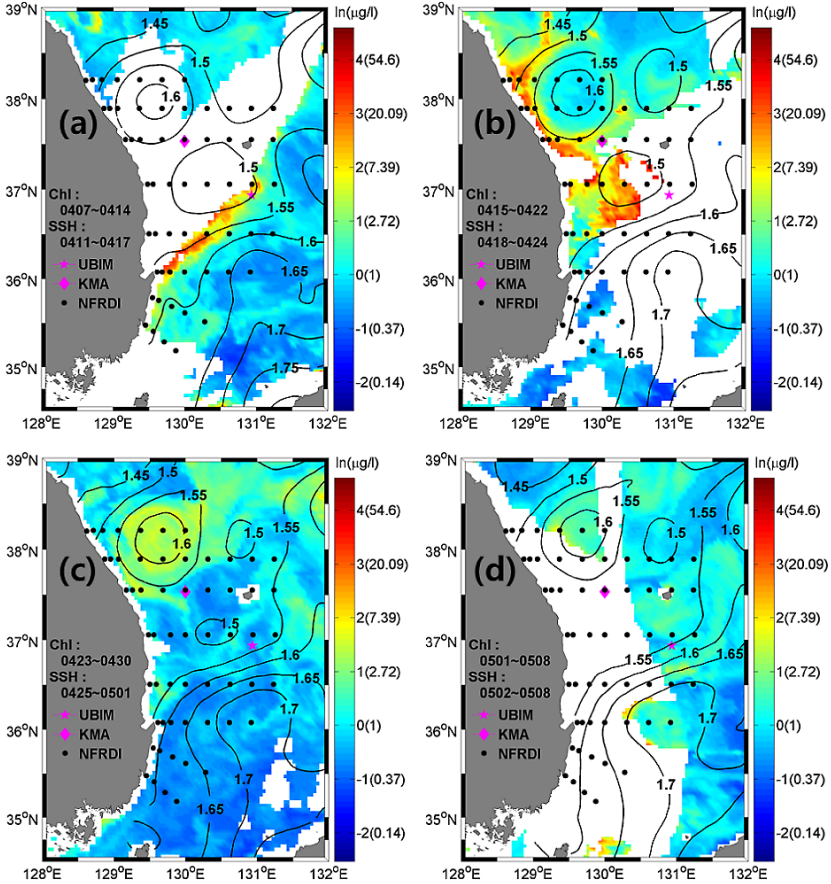

Fig. 13. 8 day composite images of MODIS chlorophyll *a* (color) during the period of buoy UBIM deployment. Composite days in month and dates are shown in each figure. 7 day composite SSH distributions close to the dates of the chlorophyll-a maps are also shown with contour lines.

BGD
10, 7831–7878, 2013

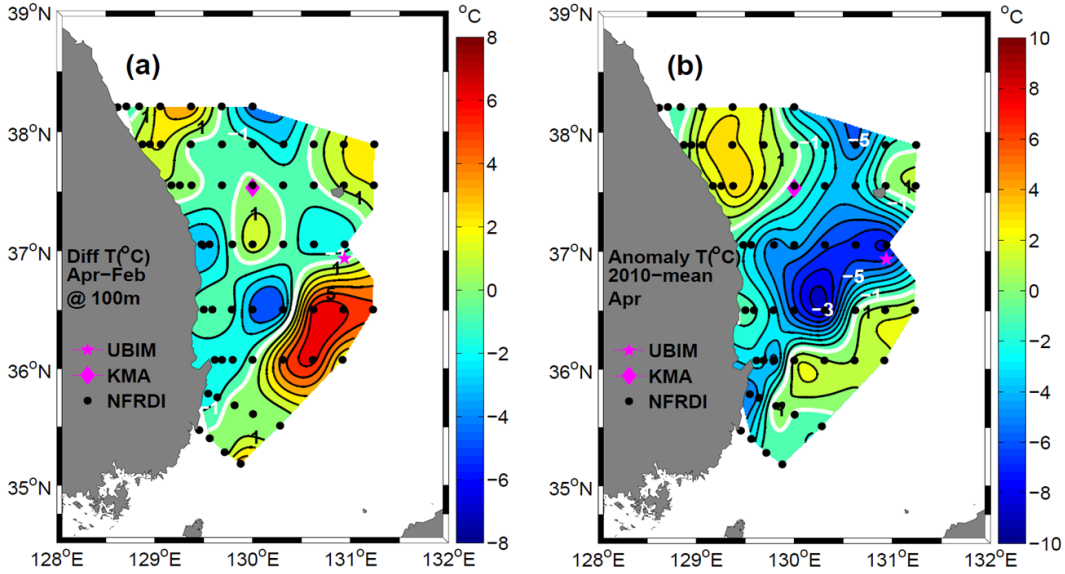

Fig. 14. (a) Temperature difference at 100 m between February and April, 2010. **(b)** Temperature anomaly at 100 m in April, 2010 with respect to the long-term mean April temperature at 100 m between 1976 and 2010. In the temperature difference map, the negative sign represents the lowering of temperature in April as compared to that in February. In the anomaly map, the negative sign indicates the cold anomaly in April, 2010 as compared to the climatological mean. White lines on both maps denote 0 values.

BGD
10, 7831–7878, 2013

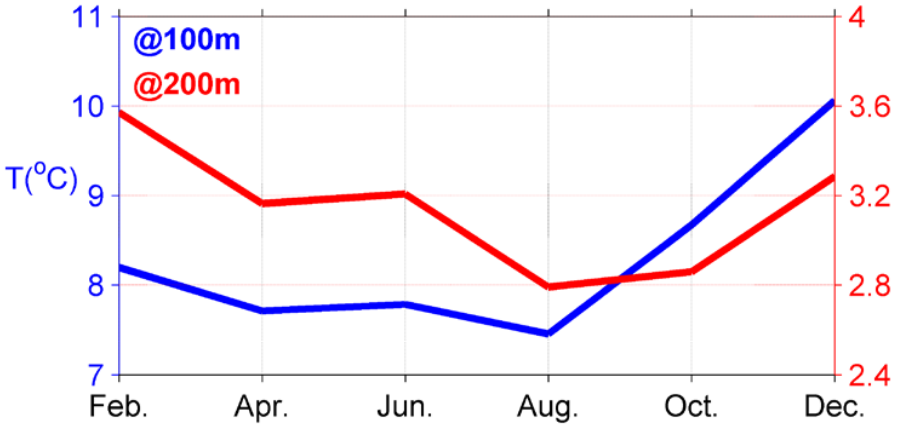

Fig. 15. Spatially averaged bi-monthly mean temperatures at 100 m and 200 m in the Ulleung Basin based on NFRDI data taken between 1976 and 2010.

BGD
10, 7831–7878, 2013